Angewandte Chemie
Eine Zeitschrift der Gesellschaft Deutscher Chemiker

Supporting Information

Structure of Nanochannel Entrances in Stopcock-Functionalized Zeolite L Composites

Gloria Tabacchi, Ettore Fois, and Gion Calzaferri**

ange_201504745_sm_miscellaneous_information.pdf

SUPPORTING INFORMATION

CONTENTS:

MODELS AND METHODS

1. Computational approach and modeling of unmodified ZL channel openings

The Zeolite L (ZL) channel opening and its site specific modifications with stopcock molecules were studied via a periodic slab approach. The model was built by cutting a slab from an optimized anhydrous ZL structure with a 1/3 Al to Si ratio and hexagonal unit cell with stoichiometry $K_9[Si_{27}Al_9O_{72}]$. The cell parameters adopted for the simulation cell were a=b=18.466 Å, c=7.476Å, γ=120°. The slab was generated by piling up three unit cells along the c axis and cutting its edges perpendicularly to the c axis. The Al-O and Si-O dangling bonds resulting from the cut were saturated with H atoms in order to mimic the ZL hydroxyl groups acting as anchoring sites for the stopcock. The stoichiometry of the slab is $K_{30}[Si_{90}Al_{30}O_{252}H_{24}]$. Periodic boundary conditions were applied in 3-dimensions, adopting a computational cell with parameters a=b= 18.466 Å, c=48.0 Å, γ=120°. The size of the c parameter allows for about 25 Å vacuum among images along the z direction. Graphical representations of the slab are reported in Figure S1.

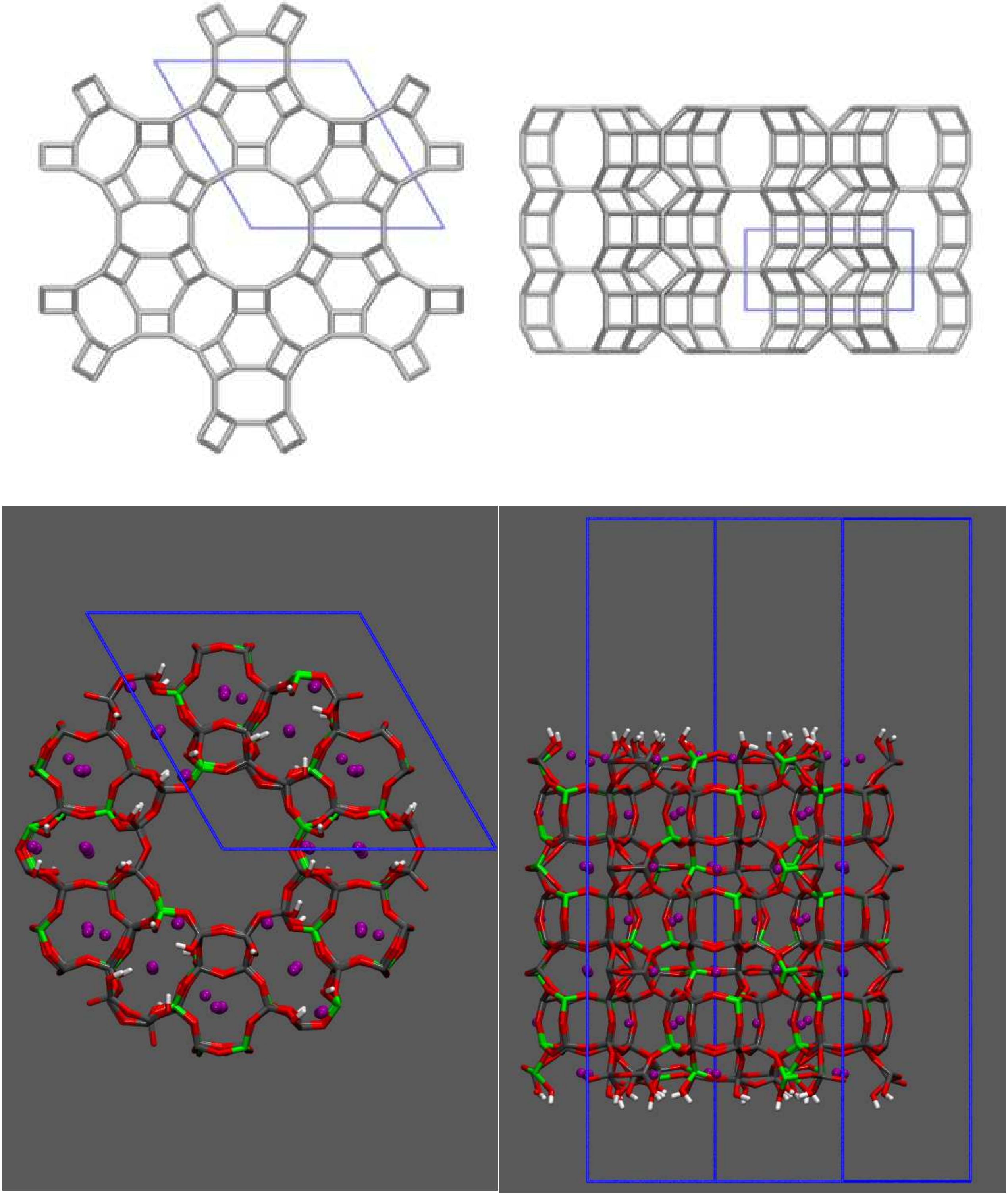

Figure S1. Top panels: the aluminosilicate framework of the ZL model, only tetrahedral sites (Si, Al) are drawn (the ZL crystallographic unit cell is shown in blue solid lines). Left: ZL model projected on the (001) plane. Right: projection perpendicular to the (001) plane showing the 3 unit cell model adopted in this work. Bottom panels: Optimized structure of the ZL model. Left: projection on the (001) plane. Right: projection perpendicular to the (001) plane. The simulation cell is shown as blue lines. Color codes: gray, Si; green, Al; red, O; purple, K; white, H.

The atomic positions of all atoms were optimized, while the cell parameters were fixed. The total charge of the system is zero. With such a geometry set up, there are two open surfaces, both with the 12-membered ring opening typical of ZL. Each surface is characterized by the presence of 12 OH groups, some belonging to Al-centered sites, others to Si-centered sites (Figure S2)

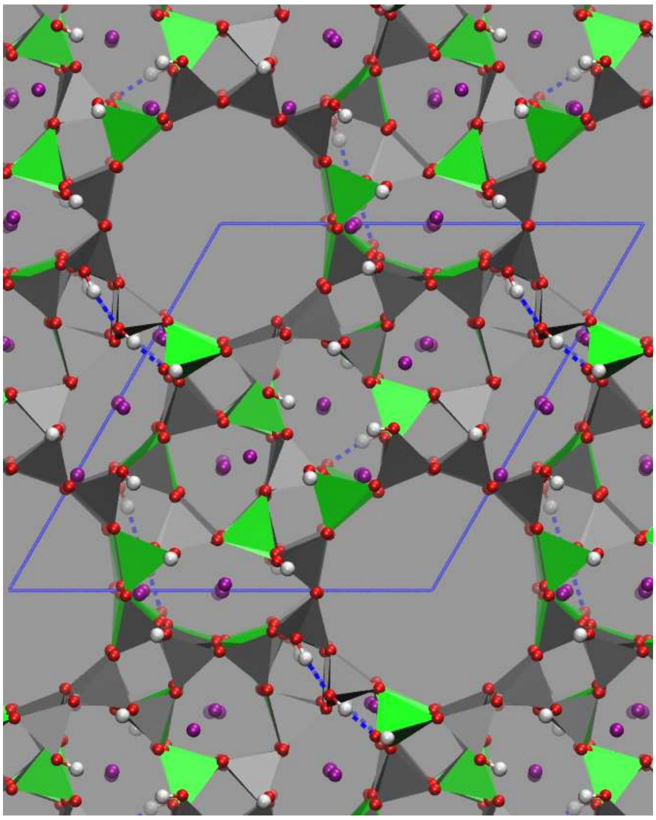

Figure S2. Representation of the channel entrances at the termination of ZL crystals in the optimized structure of the ZL model (top view). Color codes: grey, Si; green, Al; red, O; purple, K; white, H; hydrogen bonds: dashed lines; ZL unit cell: solid lines.

The PBE approximation to Density Functional Theory[1] was adopted for the electronic structure calculations, electron-nuclei interactions were treated via pseudopotentials (ultra-soft[2] for C, N, O, H, norm-conserving[3-5] for K (semi-core), Al, Si). Electronic states were expanded in a planewaves basis set up to a cutoff of 25 Ry, while electronic density was represented up to a cutoff of 200 Ry. Only the Γ point of the Brillouin zone was considered in all the calculations. Such a computational scheme for electronic structure treatment has been proved to properly describe dye-zeolite hybrids.[6] Geometry optimizations were performed on all the models via a quasi-Newton approach and stopped when maximum forces on atom positions were below 5×10^{-4} hartree/bohr. Before geometry optimization, a few picoseconds first principles molecular dynamics run was carried out at room temperature for each system. All calculations were performed with the CPMD code.[7]

2. Modeling of ZL channel openings functionalized with AETES$^+$ / IMZ$^+$ stopcocks

We chose the trialkoxysilyl cations AETES$^+$ and IMZ$^+$ as representative models for stopcocks characterized by small and bulky tail groups, respectively.

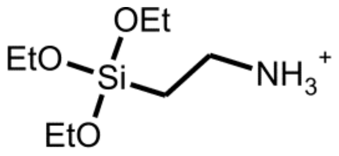

AETES$^+$

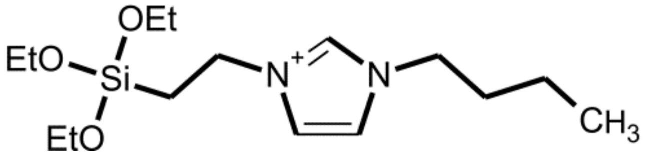

IMZ$^+$

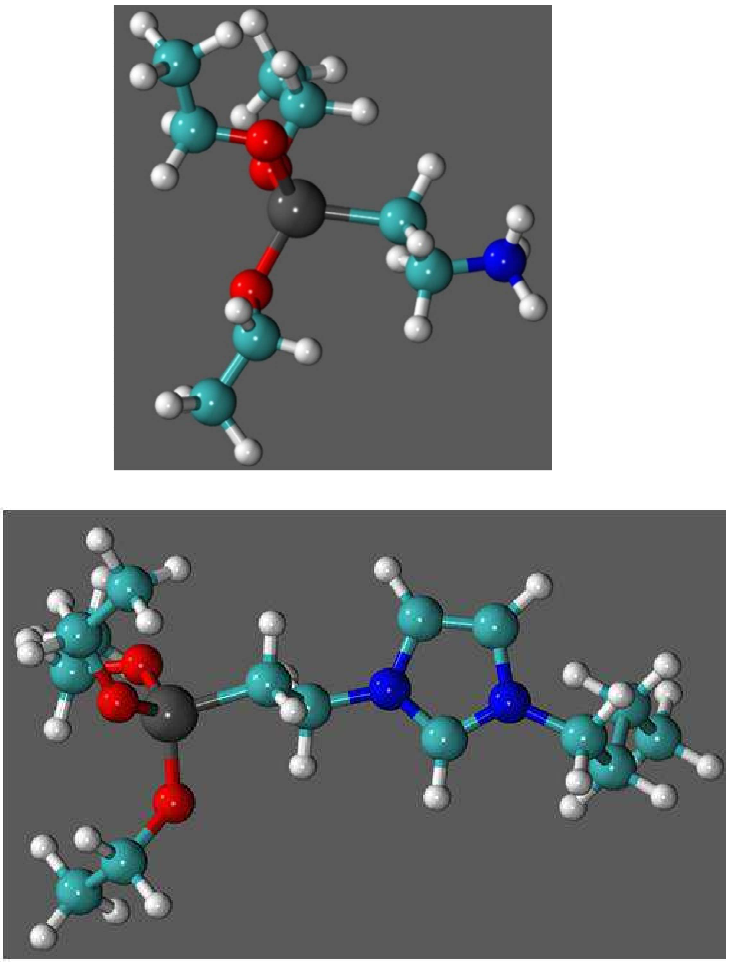

Figure S3. Optimized structures of AETES$^+$ and IMZ$^+$. Grey: Si; red: O; blue: N; cyan: C; white: H.

From these molecular stopcocks and the optimized structure of the ZL channel terminations, different stopcock-ZL model systems were designed. Such models, summarized in Table S1, are described in the following.

Table S1. Summary of adopted models and calculated stabilization energies ΔE

Model composition	type	**Description**	**ΔE**(kcal mol^{-1})
$AETES^+$-ZL·$2H_2O$	Pre	One $AETES^+$ stopcock interacting with ZL channel opening (preliminary to condensation, no covalent bonds)	-13.5
$AETES^+$-ZL·$2H_2O$	Mpod-Al	monopodal grafting of $AETES^+$ to an Al site of ZL opening (one covalent bond)	-18.1
$AETES^+$-ZL·$2H_2O$	Mpod-Si	Monopodal grafting of $AETES^+$ to a Si site of ZL opening (one covalent bond)	-15.0
$AETES^+$-ZL·$2H_2O$	Bipod	Bipodal grafting of $AETES^+$ (two covalent bonds with two adjacent Al and Si sites of the ZL channel opening)	-17.1
$AETES^+$-ZL·$4H_2O$	Mpod-Al	monopodal grafting of $AETES^+$ to an Al site of ZL opening (doubled water content)	-23.1
2·$AETES^+$-ZL·$2H_2O$	2 Mpod-Al	Two $AETES^+$ monopodally grafted to two Al sites of the opening (each $AETES^+$ forms one covalent bond with ZL)	+23.9
2·$AETES^+$-ZL·$4H_2O$	2 Mpod-Al	Two $AETES^+$ monopodally grafted to two Al sites of the opening (doubled water content)	-13.3
2·$AETES^+$-ZL·$4H_2O$	Mpod-Al + Mpod-Si	Two $AETES^+$ monopodally grafted to an Al site and to a Si site of the opening (doubled water content)	-12.0
2·$AETES^+$-ZL·$2H_2O$	Cross-linking	Cross-linking of a second $AETES^+$ to the $AETES^+$-modified system Mpod-Al	+4.4
2·$AETES^+$-ZL·$4H_2O$	Cross-linking	Cross-linking of a second $AETES^+$ to the $AETES^+$-modified system Mpod-Al (doubled water content)	-20.5
IMZ^+-ZL·$2H_2O$		monopodal grafting of IMZ^+ to an Al site of ZL opening	-1.8
IMZ^+-ZL·$4H_2O$		monopodal grafting of IMZ^+ to an Al site of ZL opening (doubled water content)	-16.4

2.1 Interaction of AETES$^+$ with ZL preliminary to grafting (Model Pre)

To investigate how a stopcock interacts with ZL in the stage preliminary to condensation, a model system (model Pre) containing ZL (Figure S2) and one AETES$^+$ ($[(EtO)_3Si(CH_2CH_2NH_3)^+]$, EtO = CH_3CH_2O, Figure S3) was designed. Specifically, the initial guess configuration for Pre was obtained starting from the optimized structure of the ZL model (Figure 2) and replacing one K$^+$ ion of the ZL channel close to the opening with AETES$^+$ in order to maintain electroneutrality. Two water molecules were included in the optimization process. The stoichiometry of the Pre system was $K_{29}[Si_{90}Al_{30}O_{252}H_{24}]\cdot[(EtO)_3Si(CH_2CH_2NH_3)^+]\cdot(H_2O)_2$ and the calculated stabilization energy ΔE was -13.5 kcal mol^{-1}. The optimized structure of Pre, shown in Figure S4, clearly evidences that only AETES$^+$ tail group enters the channel, therefore the stopcock already correctly oriented for anchoring with a covalent bond to ZL channel opening in a successive condensation step.

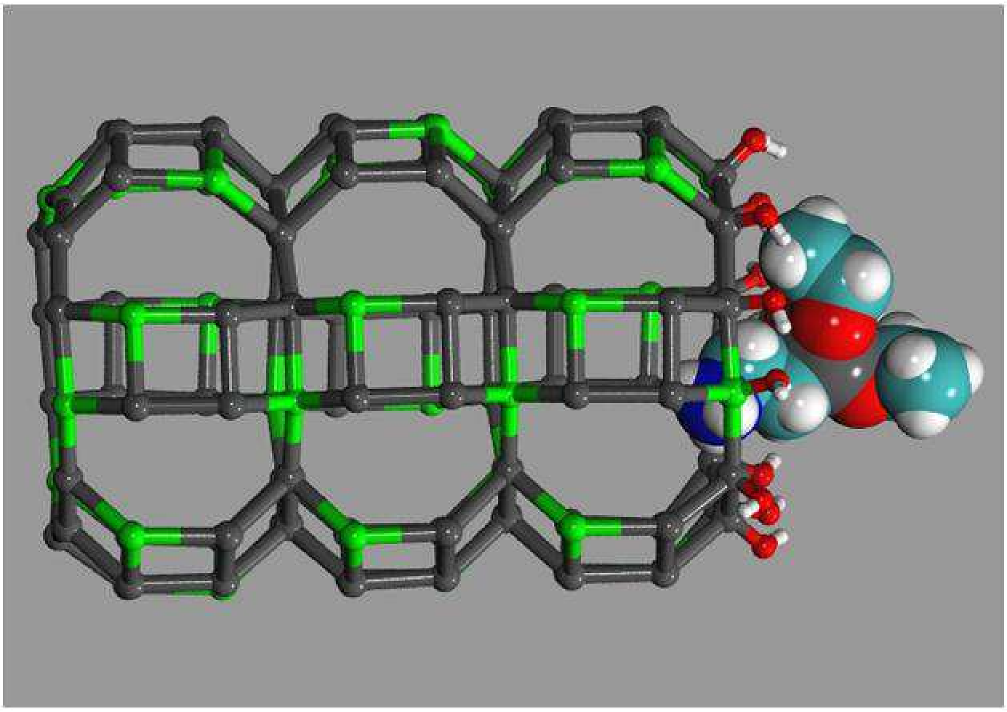

Figure S4. Side view of the optimized structure of model Pre, mimicking the interaction of stopcock AETES$^+$ with ZL (top view) preliminary to condensation. Only the tetrahedral T atoms (T=Si, Al) of the ZL framework (in ball-and-sticks), the hydroxyl groups on the ZL channel opening (in ball-and-sticks) and the atoms of AETES$^+$ (in van der Waals representation) are shown. Color codes: grey, Si; green, Al; red, O; blue, N; cyan, C; white, H.

Such AETES$^+$ orientation is stabilized by strong hydrogen bonds between the $-NH_3^+$ tail group and ZL framework oxygens, as pictured in Figure S5. Figure S5 also shows the hydrogen bonding network at the channel entrance involving ZL hydroxyl groups and water molecules.

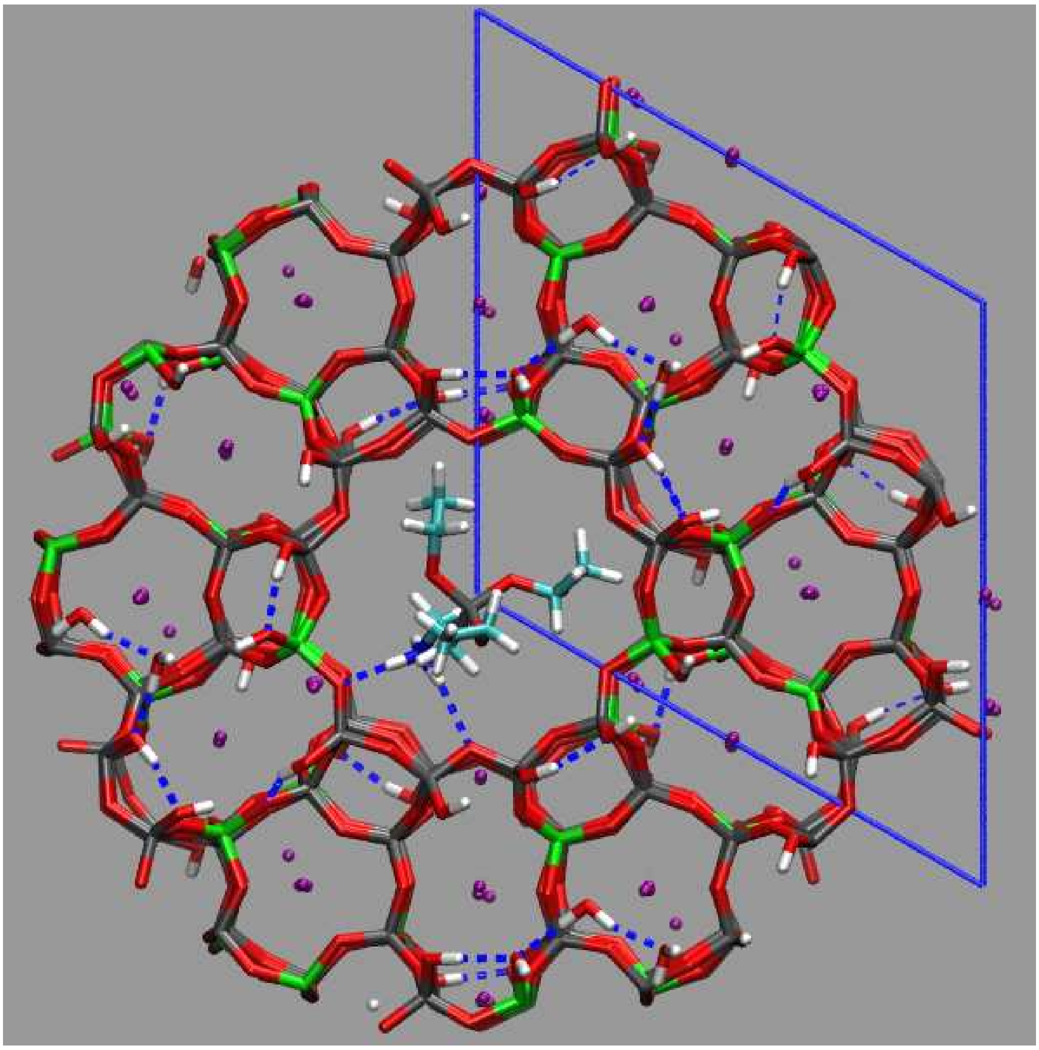

Figure S5. Top view of the optimized structure of model Pre (preliminary to condensation). All atoms of the system are shown (in ball and stick representation) . Color codes: grey: Si; green: Al; red: O; purple: K; blue: N; cyan: C; white, H. Hydrogen bonds: dashed lines; ZL unit cell: solid lines.

Covalent binding of a stopcock to ZL can lead to different types of modified zeolites. We describe in the following the models adopted to describe stopcock grafting, starting from the simplest case.

2.2 Monopodal grafting of AETES$^+$ (Models Mpod-Al, Mpod-Si)

Guess configurations for modeling AETES$^+$-ZL adducts characterized by one monopodally grafted AETES$^+$ (*i.e.*, one stopcock-zeolite covalent bond), were obtained by formally cleaving one ethoxy (EtO) group from the stopcock and one –H atom from an AlO-H (or from a SiO-H) hydroxyl located on the ZL channel entrance. In this way, we obtained two models, Mpod-Al and Mpod-Si, mimicking the grafting of AETES$^+$ to an Al or a Si site, respectively. Geometry optimization of the guess configurations was then performed. As done for model Pre, two water molecules were included in the optimization process. The stoichiometry of these AETES$^+$-ZL covalent models was $K_{29}[Si_{90}Al_{30}O_{252}H_{23}]\cdot[(EtO)_2Si(CH_2CH_2NH_3)^+]\cdot(H_2O)_2\cdot(EtOH)$. The optimized geometry of the most stable system Mpod-Al is shown in Figure S6 (side view) and S7 (top view). Figure S7 shows the hydrogen bond network of water and the hydrogen bonds between the stopcock and ZL

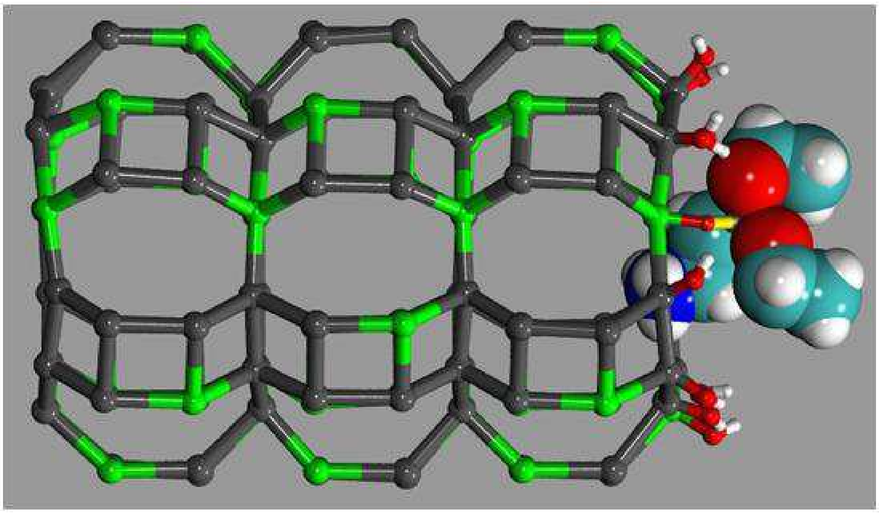

Figure S6. Side view of the optimized structure of Mpod-Al, mimicking one AETES$^+$ stopcock monopodally grafted to an Al site of the ZL channel entrance (top view) . Color codes as in Figure S4. The condensation bond is highlighted in yellow.

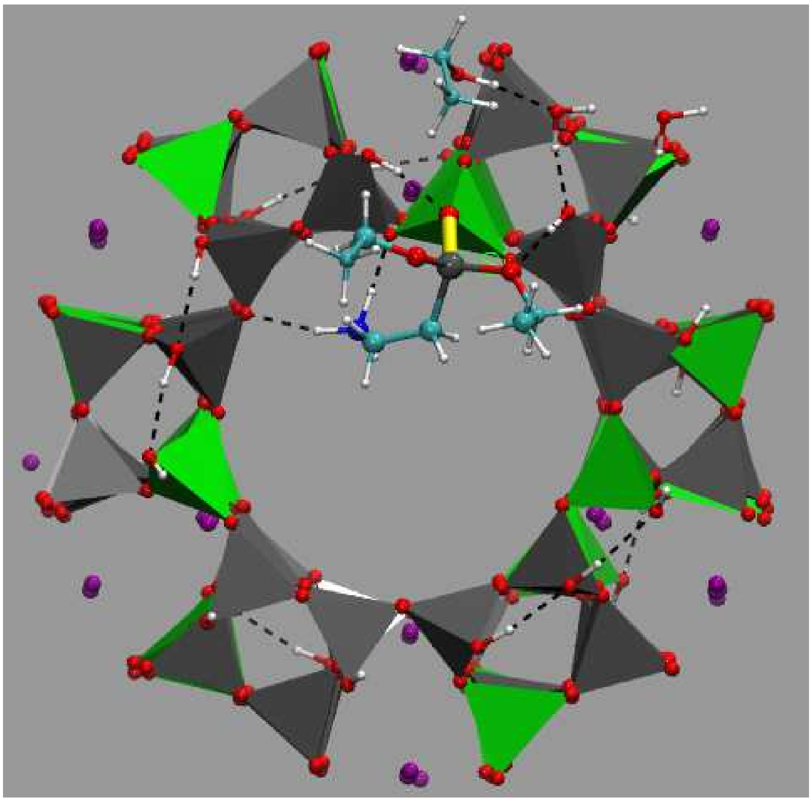

Figure S7. Top view of the optimized structure of model Mpod-Al. All atoms of the system are shown. ZL framework atoms are represented as tetrahedra. The ZL charge compensating potassium cations, AETES$^+$, water and ethanol are shown in ball and stick representation. The AETES$^+$-ZL condensation bond is highlighted in yellow. Color codes: grey: Si; green: Al; red: O; purple: K; blue: N; cyan: C; white, H. Hydrogen bonds: black dashed lines.

The effect of water on the stability of the stopcock-modified system Mpod-Al was investigated by adding two water molecules to the corresponding optimized structure, leading therefore to a system with $K_{29}[Si_{90}Al_{30}O_{252}H_{23}]\cdot[(EtO)_2Si(CH_2CH_2NH_3)^+]\cdot(H_2O)_4\cdot(EtOH)$ stoichiometry. Geometry optimization was then performed leading to a structure (not shown) characterized by very similar geometrical parameters and AETES$^+$ positioning. The stabilization energy was -23.14 kcal mol^{-1} .

2.3 Bipodal grafting of AETES$^+$ to ZL

Bipodal grafting of AETES$^+$ corresponds to a situation where two condensation bonds are formed between the stopcock and two hydroxyl groups on the ZL channel opening. In this case, the stoichiometry of the model system Bipod was $K_{29}[Si_{90}Al_{30}O_{252}H_{22}]\cdot[(EtO)SiR^+]\cdot(H_2O)_2\cdot(EtOH)_2$, due to the cleavage of two EtO– groups from the stopcock and two –H from the zeolite channel entrance. Geometry optimization led to an AETES$^+$ stopcock bipodally grafted to ZL.

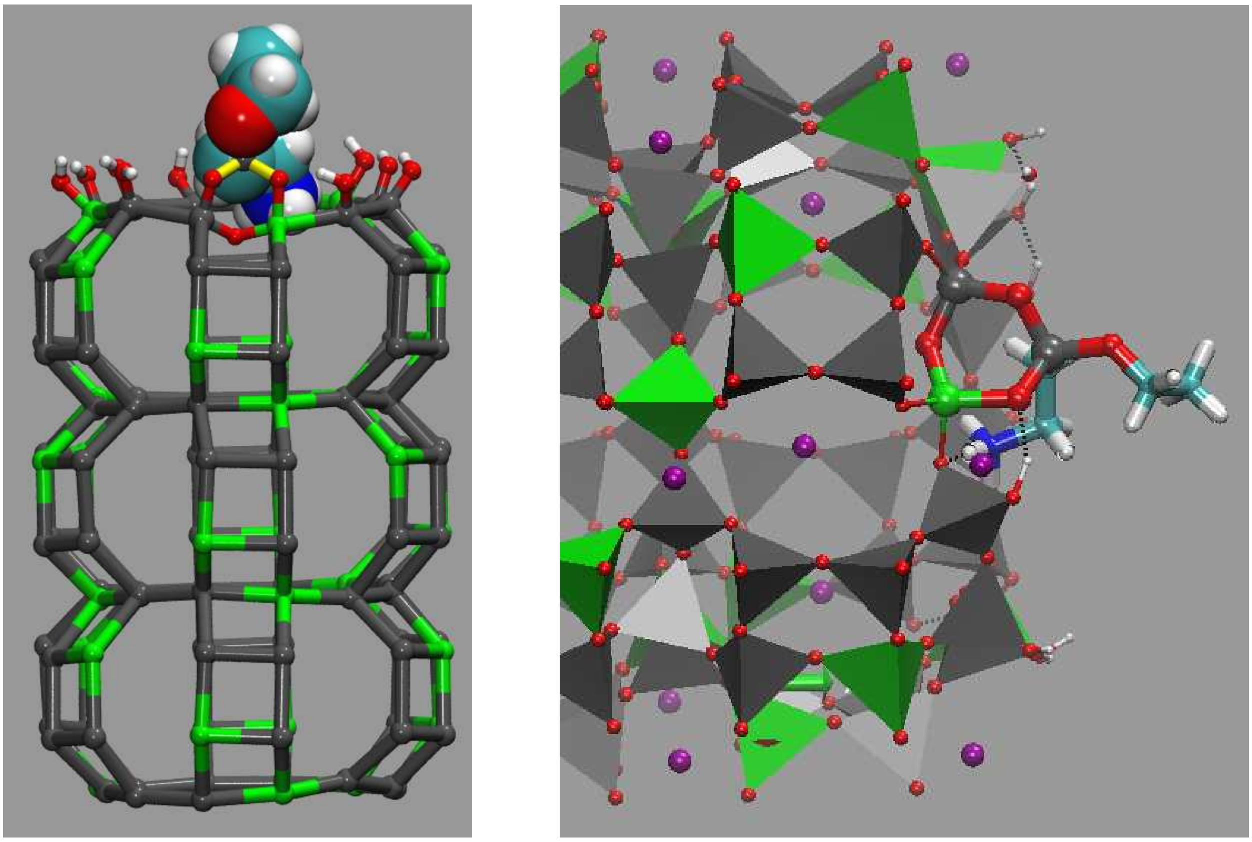

Figure S8. Left: side view of the optimized structure of model Bipod. Color codes as in Figure S4. The two AETES$^+$-ZL condensation bond forming the 3T-ring are highlighted in yellow. Right: Enlargement of the 3T-ring. To highlight the ring, ZL framework atoms are shown as tetrahedra and stopcock atoms as ball-and sticks. ZL charge compensating cations are also shown (purple spheres). Hydrogen bonds: dashed lines.

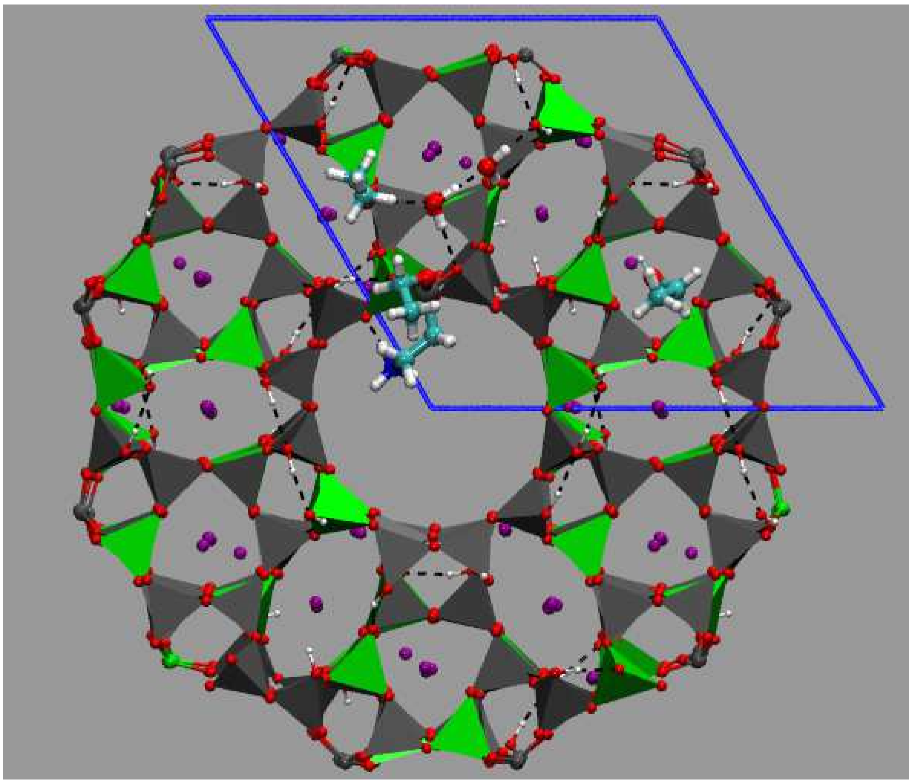

Figure S9. Top view of the optimized structure of model Bipod. All atoms of the system are shown. ZL framework atoms are represented as tetrahedra. The ZL charge compensating K^+ cations, $AETES^+$, water and ethanol are shown in ball and stick representation. Atom color codes as in Figure S7. Hydrogen bonds: black dashed lines; ZL unit cell: blue solid lines.

2.4 Grafting of two $AETES^+$ molecules on two distinct ZL sites

Full plugging of the ZL channel entrances might be accomplished by grafting two $AETES^+$ molecules on two distinct ZL sites, i.e. by formally cleaving one or two ethoxy groups from each stopcock and, correspondingly, one or two –H atoms from hydroxyl groups on the ZL channel entrance. Since both monopodal and bipodal grafting of one $AETES^+$ stopcock led to stable modifications, different modified structures may in principle arise from the anchoring of two $AETES^+$ on the channel entrance: both may be grafted monopodally, both bipodally, or one monopodally and the other one bipodally. However, bipodal modifications are energetically less favorable than the monopodal ones and are characterized by a strained structural motif (the 3-membered ring). In view of these reasons, only the case of two monopodally grafted $AETES^+$ was considered. Two models were built starting from Mpod-Al, which was the most stable structure calculated for the grafting of a single $AETES^+$ stopcock on ZL. The OH group for grafting the second $AETES^+$ was selected from either an Al or a Si site of the opening. Effects of hydration were also studied, by performing optimizations with 2 and with 4 water molecules *per* cell. The stoichiometry was $K_{28}[Si_{90}Al_{30}O_{252}H_{22}]\cdot[(EtO)_2SiR^+]_2\cdot(H_2O)_n\cdot(EtOH)_2$, with n=2, 4.

The most stable system was the one with both AETES$^+$ grafted to Al sites and with 4 H_2O molecules (Figures S10, S11). The distances between the N atoms of the two grafted stopcocks amounts to 5.16 Å. Such value is comparable with the shortest distance between charge compensating K^+ cations in the unmodified ZL (~5.5 Å), in line with the fact that the stopcock R-NH_3^+ groups have replaced two ZL charge compensating cations to maintain electroneutrality. The rather close separation between positive-charge-bearing moieties should result in a repulsive contribution to the stopcock-zeolite interaction. Water molecules are however located between the tails, so as to screen the positive charges of the R-NH_3^+ groups (Figure S11).

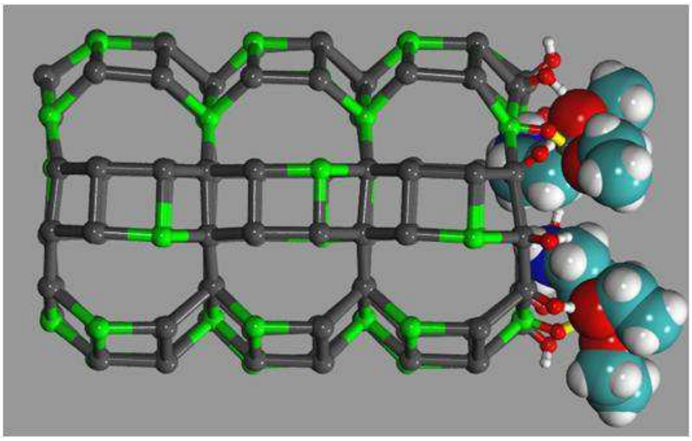

Figure S10. Side view of the most stable optimized structure of the adduct mimicking the grafting of two AETES$^+$ on two distinct Al sites of ZL. Color codes as in Figure S4. The condensation bonds are highlighted in yellow.

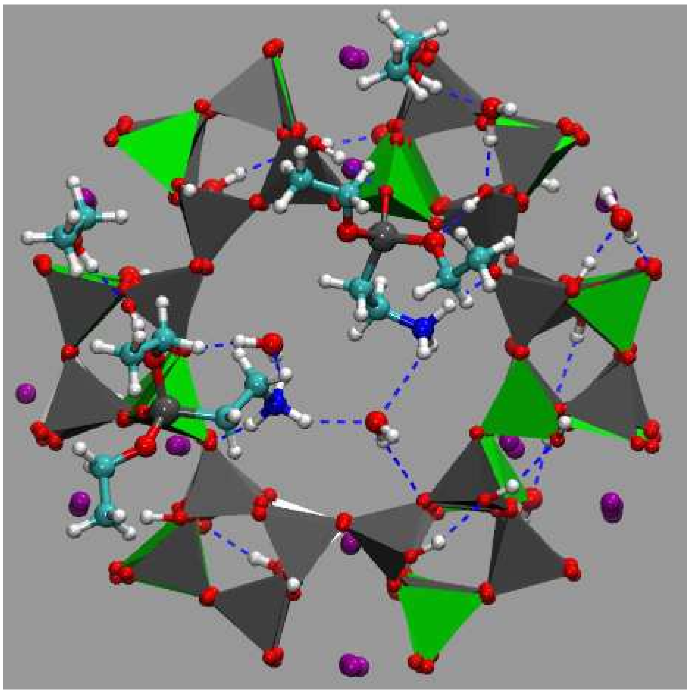

Figure S11. Top view of the structure with two AETES$^+$ grafted to two Al sites. All atoms of the system are shown. ZL framework atoms are represented as tetrahedra. The ZL charge compensating K^+ cations, AETES$^+$, water and ethanol are shown in ball and stick representation. Atom color codes as in Figure S7. Hydrogen bonds: blue dashed lines.

2.5 Cross-condensation (binding of AETES to AETES$^+$-functionalized ZL)

Cross-linking at the ZL channel opening was investigated by adopting a stopcock of formula O-$[Si(EtO)_2R]_2H^+$, where R is the ethylamine ($-CH_2CH_2NH_2$) moiety, characterized by only one protonated amino group. Such a species formally derives from the cross-condensation of a neutral AETES $[(EtO)_3Si(CH_2CH_2NH_2)]$ with a charged one $[(EtO)_3Si(CH_2CH_2NH_3]^+$. Only the grafting of this moiety at an Al-OH group of ZL was considered, with the formal release of a EtOH species which was included in the calculation. This system mimics the product of the cross-linking reaction of a neutral AETES to the AETES$^+$-functionalized zeolite. Also for this system, solvation by two and four water molecules was considered. Only in the latter case geometry optimization led to a stable cross-linked ZL adduct, represented in Figures S12 and S13.

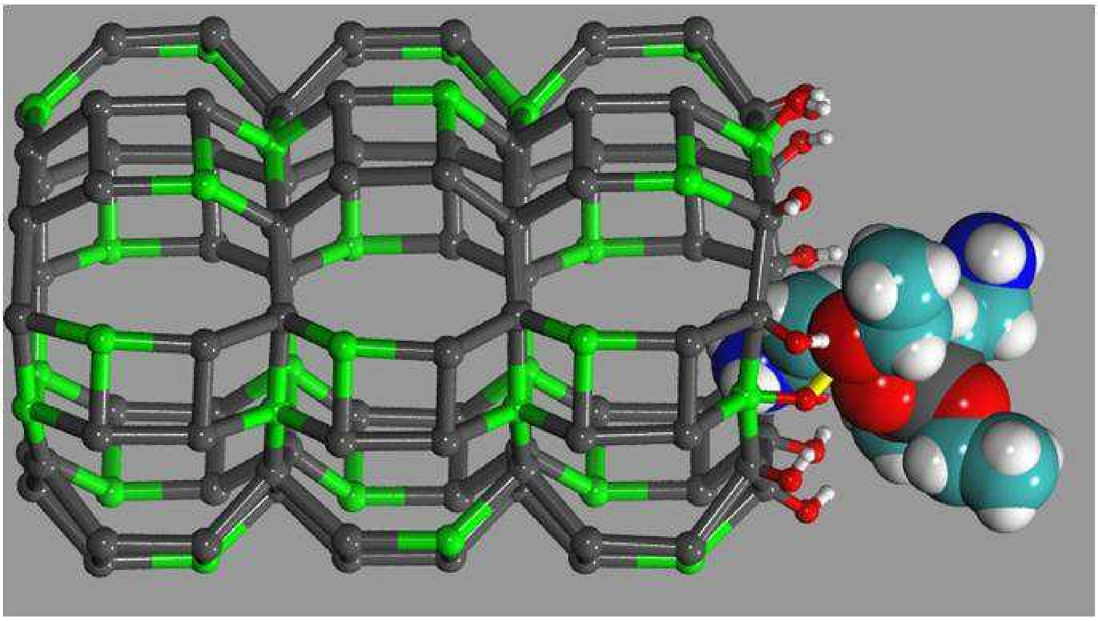

Figure S12. Side view of the optimized structure mimicking cross-linking modification of the ZL channel entrance. Color codes as in Figure S4. The condensation bond is highlighted in yellow.

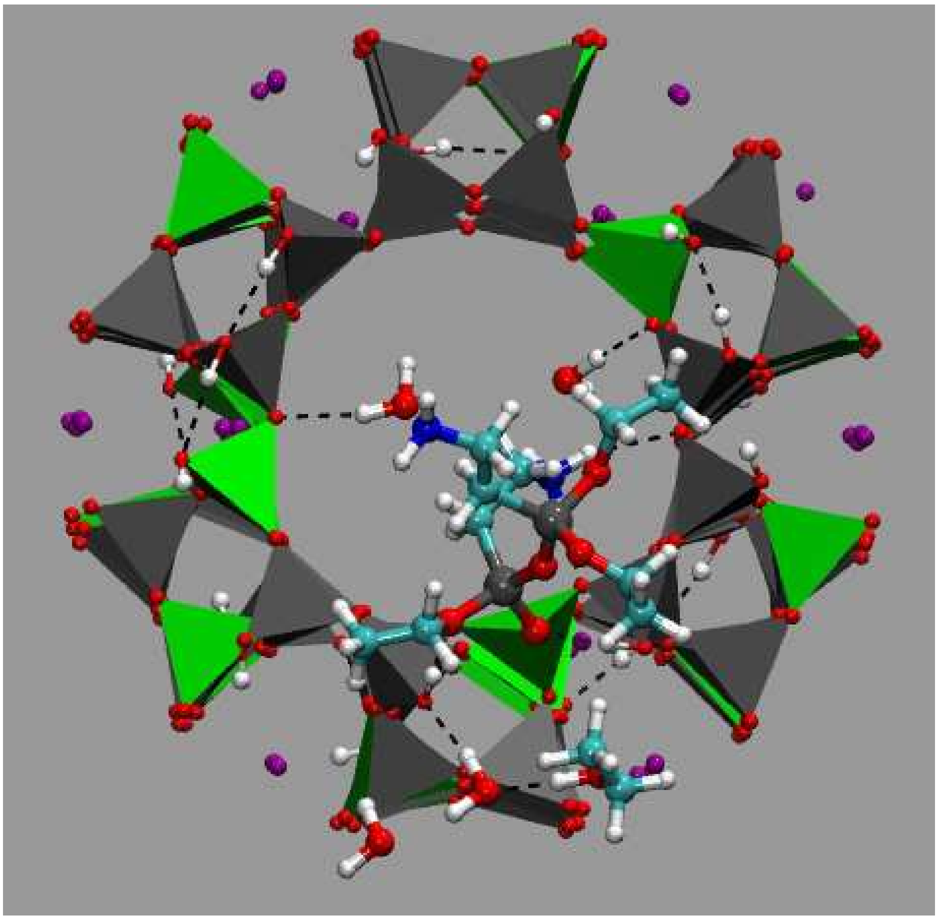

Figure S13. Top view of the optimized structure of the cross-condensation model. All atoms of the system are shown. ZL framework atoms are represented as tetrahedra. The ZL charge compensating K^+ cations, the cross-linked moiety, water and ethanol are shown in ball and stick representation. Atom color codes as in Figure S7. Hydrogen bonds: black dashed lines.

2.6 Monopodal grafting of IMZ$^+$

Since the size of IMZ$^+$ (Figure S3) is such that only one stopcock of this kind can be bound at a ZL channel opening, only a covalently bonded monopodal system mimicking the grafting of IMZ$^+$ to an Al site of the entrance was modeled. The initial guess for this system was built by following the same scheme adopted in the case of the AETES$^+$-ZL Mpod-Al model. Geometry optimization was then performed on this system, with different degrees of hydration (two and four H_2O molecules). The optimized structure calculated for the IMZ$^+$-ZL$\cdot$4H_2O model is shown in Figures S14 and S15.

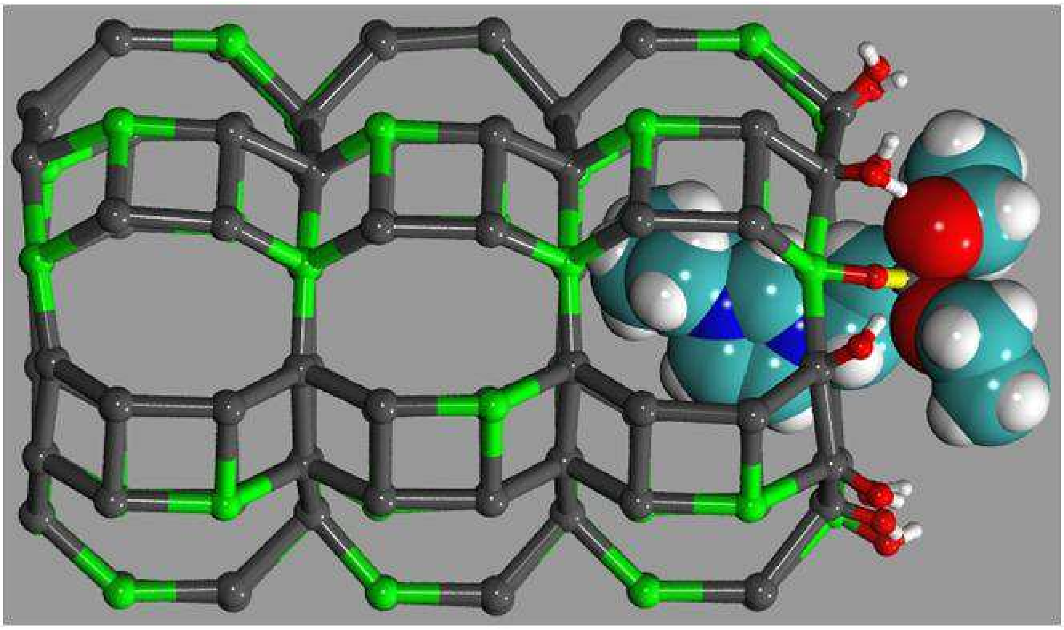
.

Figure S14. Side view of the optimized structure of model IMZ^+-$ZL \cdot 4H_2O$, mimicking ZL modification with stopcock IMZ^+. Color codes as in Figure S4. The condensation bond is highlighted in yellow.

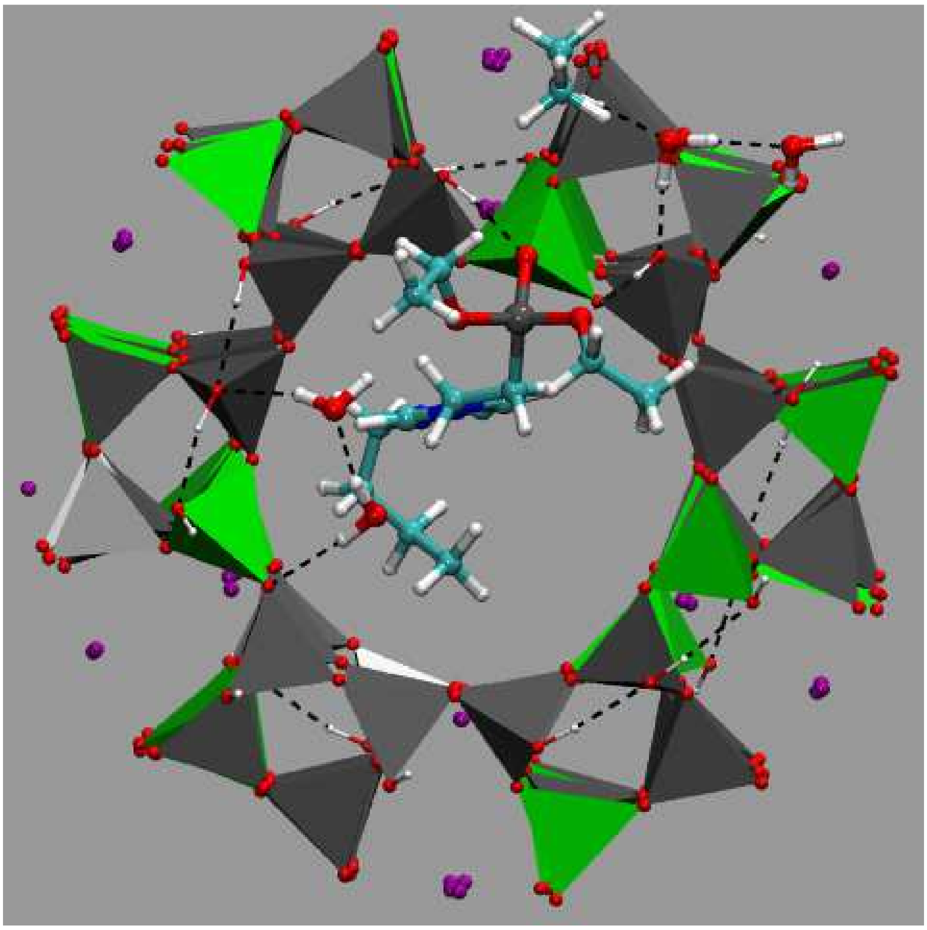

Figure S15. Top view of the optimized structure of model IMZ^+-$ZL \cdot 4H_2O$. All atoms of the system are shown. ZL framework atoms are represented as tetrahedra. The ZL charge compensating K^+ cations, IMZ^+, water and ethanol are shown in ball and stick representation. Atom color codes as in Figure S7. Hydrogen bonds: black dashed lines.

3. Calculation of the stabilization energies of the stopcock-ZL adducts.

In order to obtain stabilization energy values of the stopcock-ZL adducts, one needs the energies of the single components of the composite systems. With this aim, geometry optimizations were carried out for the AETES$^+$ ($(CH_3CH_2O)_3SiCH_2CH_2NH_3^+$), for the O-$[Si(EtO)_2(CH_2CH_2NH_2)]_2H^+$ and for the IMZ$^+$ moieties. In these cases, an isolated box of 48×48×48 Å^3 was adopted, while the other calculation parameters were the same as for the slab used for the ZL models. With the same box, the energies of a water molecule and of a K$^+$ charge compensating cation were obtained. The energies of such molecules or ions were used for calculating stabilization energies, which were obtained by subtracting from the total energy of the composite systems the energies of the components. As an example, for the case of the $K_{28}[Si_{90}Al_{30}O_{252}H_{22}]\cdot[(EtO)_2SiR^+]_2\cdot(H_2O)_4\cdot(EtOH)_2$ (namely, the system with two AETES$^+$ stopcocks and four water molecules) the stabilization energy ΔE was defined as:

$$\Delta E = E(K_{28}[Si_{90}Al_{30}O_{252}H_{22}]\cdot[(EtO)_2SiR^+]_2\cdot(H_2O)_4\cdot(EtOH)_2)$$
$$- E(K_{30}[Si_{90}Al_{30}O_{252}H_{24}]) - 2\times E((EtO)_3SiR^+) - 4\times E(H_2O) + 2\times E(K^+)$$

With such a procedure, energies of all the covalently bonded systems can be directly compared between each other and also with that of model Pre (which has no covalent bond between the stopcock and ZL). Calculated stabilization energies for all the model systems adopted in this work are summarized in Table S1.

4. Calculation of the accessibility (Connolly) surfaces.

The Connolly surfaces[8] for the stopcock-ZL models were calculated by using the corresponding optimized geometries. In all cases, the surfaces were calculated for a probe particle of 1.4 Å, adopting standard van der Waals radii. We also calculated the Connolly surfaces for two neutral dyes commonly encapsulated inside ZL for the preparation of dye-ZL composites, namely fluorenone and perylene bisimide (Figure S16). By comparing their Connolly surfaces with the ones calculated for bare ZL channel opening (Figure S16, right) and for the modified ZL systems (see Figure 4 of the main text), it is evident that these dyes have cross sections close to the bare channel entrance and that they cannot cross functionalized ZL channel openings even if the occlusion is only partial.

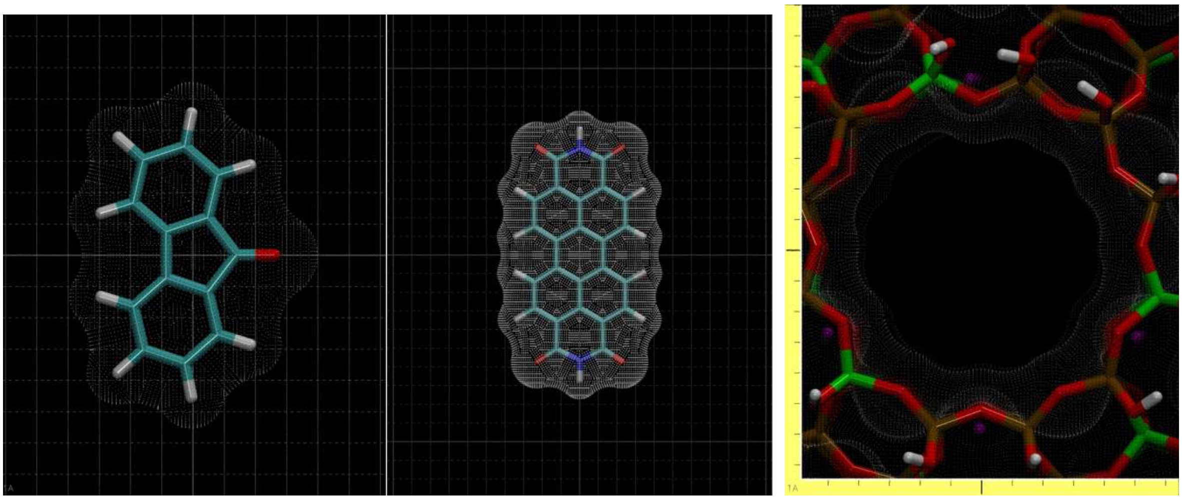

Figure S16. Connolly surfaces for fluorenone (left) and perylene bisimide (center) dyes, and for the channel opening of unmodified ZL (right panel; a 1 Å scale is drawn on the side of the picture). A 1Å×1Å grid is shown in each panel. Connolly surfaces are represented as white dots. Atom color codes: brown, Si; green, Al; red, O; magenta, K; white, H; cyan, C; blue, N.

Upon request, pdb geometry files of the optimized structures are available from the authors.

REFERENCES

[1] J.P. Perdew, K. Burke, M. Ernzerhof, *Phys. Rev. Lett.* **1996**, *77*, 3865-3868.

[2] D. Vanderbilt, *Phys. Rev. B* **1990**, *41*, 7892-7895.

[3] K. Kleinman, D.M. Bylander, *Phys. Rev. Lett.* **1982**, *48*, 1425-1428.

[4] D.R. Hamann, M. Schlüter, C. Chiang, *Phys. Rev. Lett.* **1979**, *43*, 1494−1497.

[5] N. Troullier, J.L. Martins, Phys. Rev. B **1991**, 43, 1993-2006.

[6] a) E. Fois, G. Tabacchi, G. Calzaferri, *J. Phys. Chem. C* **2010**, *114*, 10572 –10579; b)E. Fois, G. Tabacchi, G. Calzaferri, *J. Phys. Chem. C* **2012,** *116*, 16748-16799; c) E. Fois, G. Tabacchi, A. Devaux, P. Belser, D. Brühwiler, G. Calzaferri, *Langmuir*, **2013**, *29*, 9188−9198; d) L. Gigli, R. Arletti, G. Tabacchi, E. Fois, J.G. Vitillo, G. Martra, G. Agostini, S. Quartieri G. Vezzalini, *J. Phys. Chem. C* **2014,** *118*, 15732-15743.

[7] CPMD code, MPI für Festkörperforschung: Stuttgart, Germany; IBM Zürich Research Laboratory: Zürich, Switzerland, **1990−2015**, www.cpmd.org

[8] M.L. Connolly, *J.Appl. Cryst.* **1983**, *16*, 548-558.